Nano Research
2024, 17(2): 875–881

ISSN 1998-0124 CN 11-5974/O4
https://doi.org/10.1007/s12274-023-6398-z

Research Article

In vivo polydopamine coating of *Rhodobacter sphaeroides* for enhanced electron transfer

Rossella Labarile[1] (✉), Danilo Vona[2], Maria Varsalona[1,2], Matteo Grattieri[1,2], Melania Reggente[3], Roberto Comparelli[1], Gianluca M. Farinola[2], Fabian Fischer[4,5], Ardemis A. Boghossian[3], and Massimo Trotta[1] (✉)

[1] *Istituto per i Processi Chimico Fisici, Consiglio Nazionale delle Ricerche, Bari 70126, Italy*
[2] *Dipartimento di Chimica, Università degli Studi di Bari, Bari 70126, Italy*
[3] *Institute of Chemical Sciences and Engineering (ISIC), Ecole Polytechnique Fédérale de Lausanne (EPFL), Lausanne 1015, Switzerland*
[4] *Institute of Life Technologies, HES-SO Valais-Wallis, 1950 Sion, Switzerland*
[5] *Institute for Renewable Energy, HES-SO Valais-Wallis, 1950 Sion, Switzerland*

Received: 29 July 2023 / **Revised:** 4 December 2023 / **Accepted:** 5 December 2023

ABSTRACT

Recent advances in coupling light-harvesting microorganisms with electronic components have led to a new generation of biohybrid devices based on microbial photocatalysts. These devices are limited by the poorly conductive interface between phototrophs and synthetic materials that inhibit charge transfer. This study focuses on overcoming this bottleneck through the metabolically-driven encapsulation of photosynthetic cells with a bio-inspired conductive polymer. Cells of the purple non sulfur bacterium *Rhodobacter sphaeroides* were coated with a polydopamine (PDA) nanoparticle layer via the self-polymerization of dopamine under anaerobic conditions. The treated cells show preserved light absorption of the photosynthetic pigments in the presence of dopamine concentrations ranging between 0.05–3.5 mM. The thickness and nanoparticle formation of the membrane-associated PDA matrix were further shown to vary with the dopamine concentrations in this range. Compared to uncoated cells, the encapsulated cells show up to a 20-fold enhancement in transient photocurrent measurements under mediatorless conditions. The biologically synthesized PDA can thus act as a matrix for electronically coupling the light-harvesting metabolisms of cells with conductive surfaces.

KEYWORDS

bioelectronics, photosynthetic bacteria, purple bacteria, electron transfer, polydopamine, biophotovoltaics

1 Introduction

Microbial bioelectronics offers a disruptive solution to the sustainable energy problem. Such technologies benefit from the self-regulating reaction networks of a cell's metabolism. The key to unlocking these technologies lies with enabling the Faradaic exchange of electrons between the cell's metabolism and the synthetic components of the device. The electron flow in these biohybrid devices is thus regulated by the interface between the cell and the electrode [1].

Nature provides a blueprint for engineering this interface; electroactive microorganisms including bacteria as well as species of archaea, yeasts, and microalgae have evolved strategies to transfer electrons over biological membranes [2]. Certain Gram-negative bacteria [3, 4] can export charge through extracellular electron transfer (EET) that can occur either directly or via molecular intermediates [5, 6]. The underlying mechanisms of EET have been largely studied using model exoelectrogens such as *Shewanella oneidensis* MR-1 and *Geobacter sulfurreducens* [7]. However, these model organisms grow only in the presence of certain substrates, limiting their biotechnological applications. The focus has hence moved toward engineering the exoelectrogenicity of microbes that can metabolize a broader range of substrates [8–10]. Light-harvesting microbes in particular are capable of metabolizing a special range of abundant substrates, using sunlight to promote the oxidation of substrates that are otherwise energetically inaccessible [11–13].

Light-harvesting microbes like purple non-sulfur bacteria (PNSB) have a metabolic versatility that allows them to grow in different environments, under light and anoxic conditions as well as dark and oxic conditions. In the presence of light, these microbes convert solar energy into chemical energy through photosynthesis, which comprises light-harvesting proteins and photoenzymes and their cofactors, bacteriochlorophylls, carotenoid and quinones. Among PNSB, the wild type and its carotenoidless mutant strains of *Rhodobacter sphaeroides*, recently reclassified as *Cereibacter sphaeroides*, 2.4.1, and R26 respectively, have served as model organisms for studying both the molecular mechanisms of photosynthesis and the metabolism of anoxygenic photosynthesis [14]. These microbes show remarkable metabolic diversity, capable of heterotrophic growth through fermentation, as well as aerobic and anaerobic respiration. The photoheterotrophy, large substrate acceptance, and tolerance to harsh environmental conditions [15–17] make these microbes ideal for biotechnological applications.

However, the bioelectronic applications of these microbes are

Address correspondence to Rossella Labarile, r.labarile@ba.ipcf.cnr.it; Massimo Trotta, massimo.trotta@cnr.it

hampered by low power densities, with potential losses stemming from inefficient electron transfer from the cell to the electrodes. The mechanism for this inefficient EET remains an area of active research. Most applications thus often rely on the addition of exogenous redox mediators to intercept the electrons generated during photosynthesis and redirect them outside the cell, toward the electrodes [18, 19]. Unfortunately, most of these mediators show poor solubility in biological membranes and are often recalcitrant to degradation. These disadvantages limit their efficacy while also posing health and environmental risks [20, 21]. Alternative approaches for improving the EET in microbes thus range from the addition of carbon-based nanomaterials [22, 23] to the encapsulation of cells by polypyrrole [24] and polydopamine (PDA) matrices [25–27].

PDA shows strong promise as a bioinspired synthetic polymer capable of enhancing EET. It is synthesized by the oxidative self-polymerization of dopamine (DA) [28–30], benefiting from facile synthesis and functionalization [31, 32]. Importantly, PDA has a quinone- and catechol-based redox matrix that can be exploited to anchor cells on electrodes and to improve electron transport at the interface between the biological and inorganic components [26, 33]. Previous studies have demonstrated the biocompatibility of PDA matrices with photosynthetic microbes, which were able to grow in the presence of moderate concentrations of PDA under anaerobic conditions [34]. However, bioelectronic applications that exploit PDA as a conductive matrix for light-harvesting microbes are largely unexplored. Furthermore, whole-cell bioelectronic studies to date have relied on oxygenic polymerization conditions that yield non-specific, solution-phase PDA [26, 33]. These approaches overlook the advantages of metabolic-dependent polymerization for cell-specific encapsulation and for PDA association on the membranes. Such an encapsulation approach could minimize transport losses between cells while also promoting charge extraction through intimate cell contact [35].

In this study, we explore the anaerobic, metabolic PDA encapsulation of individual cells of photosynthetic bacteria for bioelectronic applications. We apply this approach to the green mutant strain *R. sphaeroides* R26 that lacks photoprotective carotenoids [36]. Consequently, this strain shows inhibited cell growth under the oxygen and light conditions typically needed for PDA polymerization. The anaerobic approach in this work thus provides a previously unexplored basis for studying the bioelectronic metabolisms of these unique microbes during photosynthesis [37–39]. Compared to bulk polymerization, the metabolic-dependent polymerization mechanism further enables the association of PDA with individual living cells. The tailored encapsulation method presented herein therefore provides a basis for enhancing the EET of individual cells in the absence of added redox mediators.

2 Experimental

2.1 Bacterial growth and functionalization

The R26 strain of *R. sphaeroides* was obtained from the German Collection of Microorganisms and Cell Cultures (DSMZ) and grown in a previously optimized medium [40]. Cell cultures were grown in biological triplicate with a starting concentration of 1 ± 0.5 × 10^9 CFU/mL (OD_{535} ~ 0.3). Oxygen was initially depleted by nitrogen insufflation. The cultures were further incubated at room temperature for 4 h in the dark to consume any residual oxygen metabolically. Following oxygen removal, the cultures were incubated at 28 °C under constant illumination by a quartz halogen lamp (80 W) placed 25 cm away from the vials. The cultures were grown in the presence of different concentrations of dopamine hydrochloride (M_W = 189.64 uma, Sigma-Aldrich) by adding 0.05, 0.1, 0.4, 1, and 3.5 mM of the monomer into the medium under anoxygenic conditions. Cells exposed to 3.5 mM dopamine were heat-inactivated and used as a negative control. Corresponding abiotic samples were also prepared by dissolving 3.5 mM of dopamine into the growth medium. At the end of every sub-inoculum, the cells were pelleted at 9000 rpm for 4 min and resuspended in 25 mM phosphate buffer 1 mM EDTA pH 7 for further characterization. Steady-state optical spectra of the samples were recorded by a Cary 5000 (Agilent) ultraviolet–visible–near infrared (UV–Vis–NIR) spectrophotometer with an internal integrating sphere for diffuse reflectance measurements (DRA 2500). Attenuated total reflectance (ATR)-Fourier transform infrared (FTIR) spectra were acquired with a Perkin Elmer Spectrum Two Spectrophotometer equipped with a 2 × 2 mm diamond crystal. Spectra were recorded in the 4000–400 cm^{-1} range with a 2 cm^{-1} resolution, using a 0.25 cm^{-1} acquisition interval with 32 scans taken for each sample.

2.2 Morphological characterization

Transmission electron microscopy (TEM) images were obtained using a JEOL JEM 1011 TEM operated at 80 kV. The samples were prepared by dropping an aliquot of the bacterial solutions after every DA addition onto a 400-mesh carbon-coated copper grid and air drying. The thickness of the PDA layer coating was calculated from different samples. A minimum of 10 surfaces/bacterium was used for the analysis, which was performed with ImageJ software. At the end of the gradual DA addition, the bacteria were exposed to a mixture of 2% paraformaldehyde and 2% glutaraldehyde in 10 mM phosphate-buffered saline (PBS) containing 150 mM NaCl (pH 7.2) for 2 h at room temperature, washed twice with 10 mM PBS, and fixed at room temperature for 2 h in 1% buffered osmium tetroxide. Following fixation, the samples were dehydrated through gradual ethanol concentration exposure, concluding with pure ethanol exposure. The samples were then embedded in acrylic resin LR White (Sigma, St. Louis, MO, USA), which was left to polymerize overnight at 60 °C. Ultrathin sections were cut with an ultramicrotome LKB 2128 Ultrotome equipped with a diamond knife and conventionally stained with uranyl acetate and lead citrate.

2.3 Electrochemical characterization

Pelleted cells of *R. sphaeroides* R26 exposed to dopamine were resuspended in electrolyte solution (20 mM 3-(N-morpholino)propanesulfonic acid (MOPS), 10 mM $MgCl_2$, 50 mM malic acid pH 7) for electrochemical characterization. Bacterial suspensions (1 mg/mL) were spotted on a 1 mm glassy carbon (GC) electrode and air dried. The bioanodes were sealed with a dialysis tubing cellulose membrane (Sigma Aldrich) that was previously activated in the electrolyte solution for 10 min. All the electrochemical measurements were performed in triplicate at 24 ± 1 °C using a three-electrode cell consisting of a Pt wire as the counter electrode and a Ag|AgCl (3M NaCl) reference electrode. Control experiments were performed using abiotic PDA prepared in the absence of cells (2 mg/mL under aerobic conditions [41]). The resulting PDA was spotted onto a GC electrode and exposed to continuous illumination for 3 h. The temperatures of the electrolytic solution and the electrode surface were recorded over time using both an analogic mercury thermometer and an infrared thermometer (Sovarcate). Cyclic voltammetry (CV) measurements were taken from −0.2 to 0.5 V at a scan rate of 20 mV/s. Chronoamperometry (CA) measurements were taken over three light-dark cycles of 100 s at an applied potential of 300 mV.

The third light cycle, which showed the most stabilized current, was used for the comparative analysis. All the potentials reported in this work were taken relative to the Ag|AgCl reference electrode.

3 Results and discussion

3.1 *In vivo* bacterial functionalization

R. sphaeroides cultures were grown under anaerobic conditions in the presence of different concentrations of added dopamine. The cells were incubated in the presence of 0.05, 0.1, 0.4, 1, and 3.5 mM dopamine (referred to as D1, D2, D3, D4, and D5, respectively) concentrations that were previously shown to sustain anaerobic cell growth [34]. The light absorption of the cells incubated in the presence and absence of dopamine was compared using UV–Vis absorption spectroscopy (Fig. 1(a)). As shown in the Fig. 1(a), R26 grown in the absence of dopamine shows an intense characteristic peak centered at 865 nm. This peak, which is associated with the absorption of the bacteriochlorophylls in the RC and the LH1 antenna, is sensitive to the effects of pollutants [42] and stresses in general. The same peak was observed in all samples that were grown in the presence of dopamine. These observations confirm that the cells were able to develop and sustain the formation of light-harvesting pigments in the presence of dopamine. The relative position of this peak was also compared to evaluate the extent of metabolic stress from dopamine addition. The first derivative of the plot of the absorption peak reaches zero at 865 nm, independent of the dopamine concentration (Fig. 1(b)). These results show no variation in peak shifting, and consequently metabolic stress, under the tested conditions. The overall absorption spectra further show cell scattering both in the presence and absence of dopamine, as indicated by the sloping baseline. To resolve the peak positions, an Ulbricht's sphere was used to remove the effects of cell scattering. As shown in Fig. 1(c), the resolved spectra show distinct absorption peaks at 380 and 590 nm, in addition to the 865 nm peak. These additional peaks correspond to bacteriochlorophylls, as reported in previous studies [43]. Though the samples showed different peak intensities for different dopamine concentrations, no trend was observed with the varying concentrations. Nonetheless, all samples showed comparable peak ratios (Table 1), indicating that the integrity of the photosynthetic apparatus of the carotenoidless mutant strain remained intact.

FTIR-ATR spectroscopy was further used to confirm the *in situ* anoxygenic polymerization of PDA following dopamine addition (Fig. 2(a)). As shown in previous studies, the dopamine can polymerize in the absence of oxygen when incubated with metabolically active cells [34]. Under these conditions, the cells may contribute an alternative oxidative pathway for PDA polymerization. Consistent with these results, the *R. sphaeroides* cells exposed to dopamine show a signal between 1560 and 1566 cm^{-1}, corresponding to the stretching and bending vibration [44] (Fig. 2(b)). The characteristic peak around 1598 cm^{-1} is also indicative of DA oxidation to PDA [45]. This peak is absent in the R26 sample grown without dopamine. In addition, all the biological samples (both with and without dopamine) exhibit peaks between 3450–3230 cm^{-1} corresponding to –OH and –NH stretching and a peak around 1600 cm^{-1} corresponding to protein carboxyl groups.

3.2 Morphological characterization

The PDA deposition was further characterized by TEM. Micrographs of ultrathin sections of *R. sphaeroides* cells grown in the presence of dopamine show a PDA nanoparticle coating surrounding the membranes of individual cells (Fig. 3). These observations agree with previous studies that have shown anoxygenic PDA formation from cell activity [34]. In addition, the PDA nanoaggregates were largely observed near the cells, consistent with a mechanism that is based on metabolic activity.

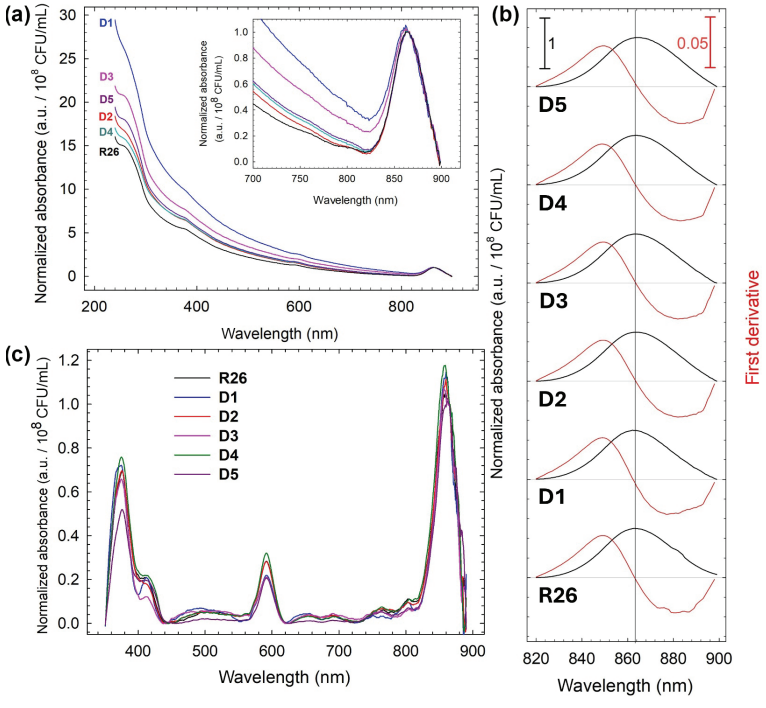

Figure 1 Spectroscopic characterization of *R. sphaeroides* R26 cells exposed to dopamine at different concentrations. (a) UV–Vis spectra of unexposed R26 cells (R26), and R26 cells exposed to 0.05 mM (D1), 0.1 mM (D2), 0.4 mM (D3), 1 mM (D4), and 3.5 mM (D5) of dopamine plotted as normalized absorbance at 10^8 CFU/mL and at the characteristic peak of *R. sphaeroides* R26 (at 865 nm) to estimate of the antenna size for an equivalent number of cells. The inset focuses on the 820–900 nm range. (b) Absorbance of R26, D1, D2, D3, D4, and D5 samples normalized by the CFU/mL (on the left) with the corresponding first derivative (on the right). The vertical line represents the wavelength at which the first derivative is equal to zero in the R26 sample. (c) UV–Vis–NIR spectra of R26, D1, D2, D3, D4, and D5 recorded with an Ulbricht's sphere.

Table 1 Peak ratio in reflectance spectra

Peak ratio	R26	D1	D2	D3	D4	D5	Average ratio
865/592	3.7	5.4	3.9	5.0	3.7	4.8	4.4±1.2
865/375	1.5	1.6	1.6	1.6	1.6	1.9	1.6±0.3

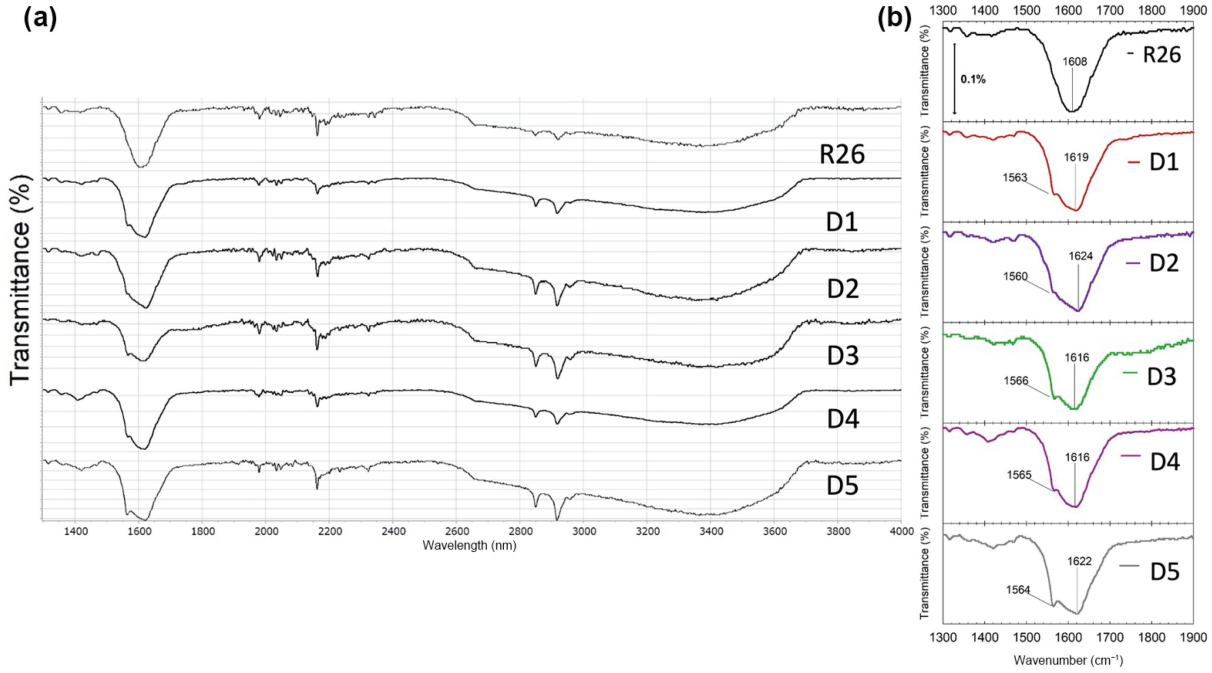

Figure 2 ATR-FTIR spectra of R26 exposed to dopamine. (a) Spectra (1300–4000 cm^{-1}) of unexposed R26 cells (R26), and R26 cells exposed to 0.05 mM (D1), 0.1 mM (D2), 0.4 mM (D3), 1 mM (D4), and 3.5 mM (D5) of dopamine. (b) Spectra (1300–1900 cm^{-1}) focused around the PDA peak.

The concentration-dependent formation of the PDA nanoaggregates was also examined using whole-cell TEM imaging (Fig. 4). At low dopamine concentrations (D1–D2), the images show negligible formation of dark nanoaggregates, suggesting limited PDA formation. The micrographs show the onset of nanoparticle layers beginning to form on the cell membrane (Fig. 4, D2, bottom panel). These observations are consistent with a concentration-dependent mechanism that relies on cell surface deposition. By contrast, dopamine concentrations above 0.4 mM (D4–D5) show more pronounced nanoaggregates that appear to increase in size with concentration, achieving nanoaggregates up 50 nm in diameter in the presence of 3.5 mM dopamine. The size of these nanoaggregates is comparable to that of abiotic PDA synthesized in the presence of oxygen (Fig. S1 in the Electronic Supplementary Material (ESM)). The increasing dopamine concentrations also lead to an overall increase in the thickness of the layers, increasing from 100 ± 20 nm for D3 to 180 ± 30 nm for D5 (Fig. S2 in the ESM). The deposition of thick PDA layers can diminish cell growth and viability, as the PDA may limit light absorption. Recent studies, however, have shown sustained cell growth for concentrations up to at least 1 mM dopamine [34, 46]. These results indicate a basis for examining the cell exoelectrogenicity in the presence of moderate PDA concentrations.

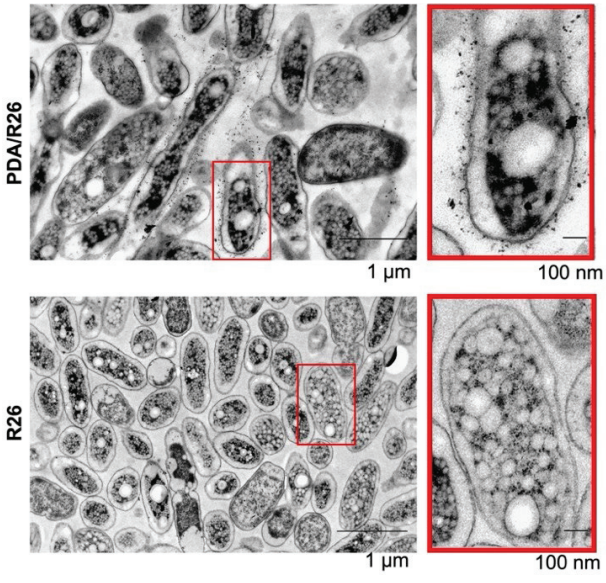

Figure 3 TEM micrographs of R26 in the presence and absence of PDA. Ultrathin sections of PDA-functionalized R26 cells (top) were taken in the presence of 3.5 mM dopamine. Ultrathin sections of bare R26 cells (bottom) were taken in the absence of added dopamine. Red boxes highlight selected cells that are enlarged in the right panels.

3.3 Electrochemical characterization

The effect of the PDA coating on the exoelectrogenicity of the cells was examined using a three-electrode setup. The setup consisted of a GC working electrode, a Pt counter electrode, and Ag|AgCl reference electrode. The photothermal effects of the PDA were first characterized in the absence of cells by monitoring the temperature increase of the PDA-coated GC electrode relative to the bulk solution under continuous 3-h illumination (Fig. S3 in the ESM). Under these conditions, the electrochemical cell temperature increased from 24.2 ± 0.1 to 26.3 ± 0.1 °C. Importantly, the electrode surface showed no significant difference in temperature compared to the bulk. These observations confirm negligible photothermal heating from the PDA even under extended illumination conditions in the presence of excess PDA. Electrochemical measurements were performed without the addition of exogenous redox mediators to characterize direct electron transfer. Compared to the bare GC electrode, the electrode incubated with R26 cells shows a small redox peak

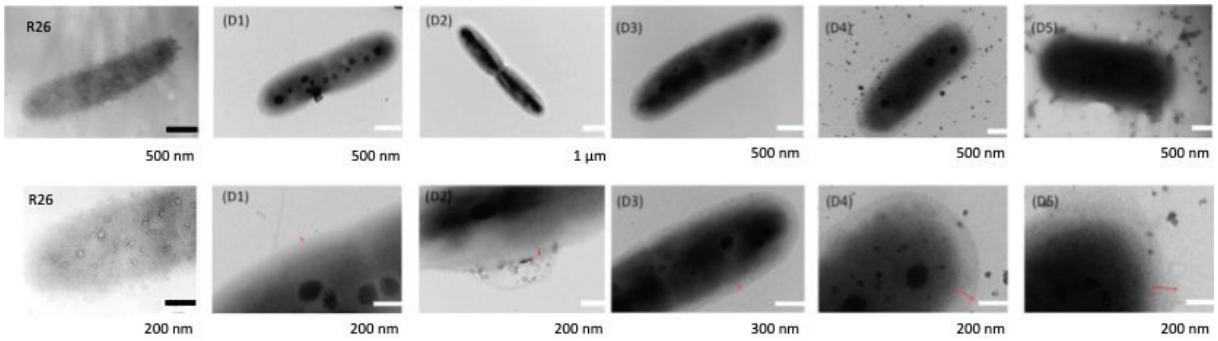

Figure 4 Whole-cell TEM images of R26 cells exposed to increasing concentrations of dopamine. Images were obtained for cells in the absence (R26, left) and presence of 0.05 mM (D1), 0.1 mM (D2), 0.4 mM (D3), 1 mM (D4), and 3.5 mM (D5) of dopamine. Both low (top) and high (bottom) magnifications are shown.

around 0.23 V (Fig. S4 in the ESM). When incubated in the presence of 3.5 mM dopamine (D5), the sample shows a more pronounced peak at 300 mV, corresponding to catechol reduction [47]. The CA measurements performed at this applied potential show an increased photoresponse of the cells with increasing PDA (Fig. 5(a)). Although photoresponses are also observed for negative controls including uncoated cells, heat-inactivated cells, and abiotic PDA electrodes prepared using D5-equivalent concentrations of dopamine (3.5 mM) (Fig. 5(b)), these responses are substantially diminished compared to the D3, D4, and D5 samples of R26 with PDA.

These observations thus confirm a contribution that stems from the metabolic activity of the living cells.

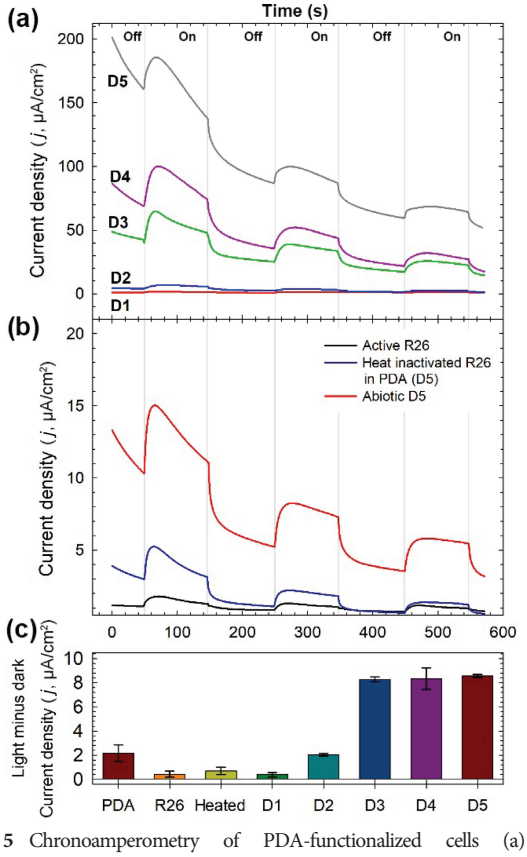

Figure 5 Chronoamperometry of PDA-functionalized cells (a) CA measurements taken under alternating light and dark conditions at 100 s intervals. PDA-functionalized R26 samples (from D1 to D5) were cyclically exposed to light. The current density was obtained by dividing current values with the geometrical area of the glassy carbon (0.0314 cm^2) (b) Chronoamperometry of untreated, active R26 cells (black), heat-inactivated R26 cells after encapsulation at D5 concentrations (blue) and abiotic electrodes prepared at D5 concentrations (red) produced by dissolving 3.5 mM of dopamine in *R. sphaeroides* growth medium. Samples were cyclically exposed to dark and light conditions. (c) Histogram representing the current difference under dark and light conditions during the third cycle.

A comparison of the baseline currents, however, also shows an increase in the dark current that increases with PDA concentration. This trend suggests a contribution from the PDA as well. The PDA photocurrents do not show a monotonic increase while under illumination, nor do the PDA-coated cells show any notable delay in photo-response. The PDA is therefore unlikely to enhance current through photothermal effects, since illumination temperature should yield a monotonic increase (or at best leveling) of the photocurrent, and thermal effects on the cell are only observed after some delay [48]. Furthermore, the baseline current diminishes over time, likely due to the capacitive discharge of the redox-active catechol and quinone groups of the PDA. This diminution is therefore consistent with an unmediated charge transfer mechanism that relies on the redox activity of the PDA. Indeed, the cells that show the thickest PDA coating also show the greatest baseline current. The D5 cells, for example, show a coating thickness of 180 ± 30 nm, almost twice that of D3 and D4. The D5 cells also have nearly double the baseline current, suggesting a mechanism based on unmediated capacitive discharge from the PDA. By contrast, mediated measurements show sustained PDA-enhanced EET even after several hours, as they instead rely on the redox activity of added soluble mediators [46]. The greatest photocurrent, which is observed in the presence of the living cells, thus relies on the redox activity of the PDA for enhancing EET.

The difference between the light and dark currents for each of these samples was also compared based on the third illumination cycle, which showed the greatest stabilization over the course of these transient measurements (Fig. 5(c)). As shown in the Fig. 5(c), the untreated and the D1 cells show a comparable difference in the light-dark response. Though the D2 cells show a slight increase, the largest light-dark difference was observed for the highest dopamine concentrations. Interestingly, the D3, D4, and D5 samples all show comparable light-dark current differences, despite the difference in the baseline current. The comparable light-dark differences at high PDA concentrations suggest the photocurrent charge extraction to be limited by the light penetration into the PDA (Fig. S3 in the ESM). Nonetheless, even under these conditions, the samples achieve a maximum difference of 8.56 μA/cm^2, a 20-fold increase compared to unexposed R26 cells (0.42 μA/cm^2) under unmediated conditions.

4 Conclusions

This work demonstrates a metabolically driven approach for encapsulating living cells with PDA to enhance EET. This anaerobic approach was applied to the oxygen-sensitive, light-harvesting cells of *R. sphaeroides*. The *in-situ* formation of the PDA coating around single *R. sphaeroides* cells could sustain bacterial growth under anaerobic conditions [34] while promoting

electrode immobilization through improved adhesion [26, 33]. Importantly, the coated cells show a marked transient enhancement in photocurrent in the absence of added mediators. This enhancement is attributed to the improved adhesion of the cells as well as the efficient charge transfer properties of the redox–active matrix. Adhesion can improve charge collection by increasing the interaction area between the cells and abiotic components. The PDA may also improve the overall EET through more efficient charge transfer via its redox–active quinone sites. An understanding of the relative contributions of these mechanisms can be helpful in tailoring these matrices to further enhance EET. The results of this study thus lay the framework for not only synthesizing electrodes through cell activity but also tuning its synthesis to optimize EET.

Acknowledgements

M. T., R. L., D. V., and G. M. F acknowledge the useful discussion with Dr. Gabriella Buscemi. Authors wish to thank Mr. Giovanni Lasorella for his technical support. This work was funded by the Fonds National Suisse de la Recherche Scientifique, project Phosbury-Photosynthetic bacteria in Self-assembled Biocompatible coatings for the transduction of energy (Project Nr CRSII5_205925/1). M. G. acknowledges the funding from Fondazione CON IL SUD, Grant "Brains to South 2018" (project number 2018-PDR-00914).

Electronic Supplementary Material: Supplementary material (TEM micrographs of abiotic PDA sample, mean of layer thickness of R26 cells, thermal effect of the illumination on the photoelectrochemical cell, and CVs of biophotoanodes) is available in the online version of this article at https://doi.org/10.1007/s12274-023-6398-z.

References

[1] Schröder, U.; Harnisch, F.; Angenent, L. T. Microbial electrochemistry and technology: Terminology and classification. *Energy Environ. Sci.* **2015**, *8*, 513–519.

[2] Rabaey, K.; Girguis, P.; Nielsen, L. K. Metabolic and practical considerations on microbial electrosynthesis. *Curr. Opin. Biotechnol.* **2011**, *22*, 371–377.

[3] Logan, B. E. Exoelectrogenic bacteria that power microbial fuel cells. *Nat. Rev. Microbiol.* **2009**, *7*, 375–381.

[4] Lovley, D. R. Bug juice: Harvesting electricity with microorganisms. *Nat. Rev. Microbiol.* **2006**, *4*, 497–508.

[5] Reguera, G. Harnessing the power of microbial nanowires. *Microb. Biotechnol.* **2018**, *11*, 979–994.

[6] Borole, A. P.; Reguera, G.; Ringeisen, B.; Wang, Z. W.; Feng, Y. J.; Kim, B. H. Electroactive biofilms: Current status and future research needs. *Energy Environ. Sci.* **2011**, *4*, 4813–4834.

[7] Sydow, A.; Krieg, T.; Mayer, F.; Schrader, J.; Holtmann, D. Electroactive bacteria—Molecular mechanisms and genetic tools. *Appl. Microbiol. Biotechnol.* **2014**, *98*, 8481–8495

[8] TerAvest, M. A.; Zajdel, T. J.; Ajo-Franklin, C. M. The Mtr pathway of *Shewanella* oneidensis MR-1 couples substrate utilization to current production in *Escherichia coli*. *ChemElectroChem* **2014**, *1*, 1874–1879.

[9] Mouhib, M.; Reggente, M.; Li, L.; Schuergers, N.; Boghossian, A.A. Tailored extracellular electron transfer pathways enhance theelectroactivity of *Escherichia coli*. bioRxiv 2021.08.28.458029. https://doi.org/10.1101/2021.08.28.458029 (accessed Dec 4, 2023).

[10] Reggente, M.; Schurgers, N.; Mouhib, M.; Politi, S.; Antonucci, A.;Boghossian, A. A. Living photovoltaics based on recombinantexpression of MtrA decaheme in photosynthetic bacteria. bioRxiv 2023.02.28.530417. https://doi.org/10.1101/2023.02.28.530417 (accessed Dec 4, 2023).

[11] Zou, Y. J.; Pisciotta, J.; Billmyre, R. B.; Baskakov, I. V. Photosynthetic microbial fuel cells with positive light response. *Biotechnol. Bioeng.* **2009**, *104*, 939–946.

[12] Schuergers, N.; Werlang, C.; Ajo-Franklin, C. M.; Boghossian, A. A. A synthetic biology approach to engineering living photovoltaics. *Energy Environ. Sci.* **2017**, *10*, 1102–1115.

[13] Mouhib, M.; Antonucci, A.; Reggente, M.; Amirjani, A.; Gillen, A. J.; Boghossian, A. A. Enhancing bioelectricity generation in microbial fuel cells and biophotovoltaics using nanomaterials. *Nano Res.* **2019**, *12*, 2184–2199.

[14] Hunter, C. N.; Daldal, F.; Thurnauer, M. C.; Beatty, J. T. *The Purple Phototrophic Bacteria*; Springer: Dordrecht, 2009.

[15] Giotta, L.; Agostiano, A.; Italiano, F.; Milano, F.; Trotta, M. Heavy metal ion influence on the photosynthetic growth of *Rhodobacter sphaeroides*. *Chemosphere* **2006**, *62*, 1490–1499.

[16] Grattieri, M.; Labarile, R.; Buscemi, G.; Trotta, M. The periodic table of photosynthetic purple non-sulfur bacteria: Intact cell-metal ions interactions. *Photochem. Photobiol. Sci.* **2022**, *21*, 101–111.

[17] Labarile, R.; Farinola, G. M.; Varsalona, M.; Italiano, F.; Buscemi, G.; Trotta, M.; Grattieri, M. Halotolerance of Rhodobacter sphaeroides for saline and hypersaline wastewater bioremediation. In *2021 International Workshop on Metrology for the Sea; Learning to Measure Sea Health Parameters* (*MetroSea*), Reggio Calabria, 2021, pp 37–42.

[18] Reggente, M.; Politi, S.; Antonucci, A.; Tamburri, E.; Boghossian, A. A. Design of optimized PEDOT-based electrodes for enhancing performance of living photovoltaics based on phototropic bacteria. *Adv. Mater. Technol.* **2020**, *5*, 1900931.

[19] Hasan, K.; Yildiz, H. B.; Sperling, E.; Conghaile, P. Ó.; Packer, M. A.; Leech, D.; Hägerhäll, C.; Gorton, L. Photo-electrochemical communication between cyanobacteria (*Leptolyngbia* sp.) and osmium redox polymer modified electrodes. *Phys. Chem. Chem. Phys.* **2014**, *16*, 24676–24680.

[20] Beauzamy, L.; Delacotte, J.; Bailleul, B.; Tanaka, K.; Nakanishi, S.; Wollman, F. A.; Lemaître, F. Mediator-microorganism interaction in microbial solar cell: A fluo-electrochemical insight. *Anal. Chem.* **2020**, *92*, 7532–7539.

[21] Gemünde, A.; Lai, B.; Pause, L.; Krömer, J.; Holtmann, D. Redox mediators in microbial electrochemical systems. *ChemElectroChem* **2022**, *9*, e202200216.

[22] Antonucci, A.; Reggente, M.; Roullier, C.; Gillen, A. J.; Schuergers, N.; Zubkovs, V.; Lambert, B. P.; Mouhib, M.; Carata, E.; Dini, L. et al. Carbon nanotube uptake in cyanobacteria for near-infrared imaging and enhanced bioelectricity generation in living photovoltaics. *Nat. Nanotechnol.* **2022**, *17*, 1111–1119.

[23] Liu, S. R.; Yi, X. F.; Wu, X. E.; Li, Q. B.; Wang, Y. P. Internalized carbon dots for enhanced extracellular electron transfer in the dark and light. *Small* **2020**, *16*, 2004194.

[24] Song, R. B.; Wu, Y. C.; Lin, Z. Q.; Xie, J.; Tan, C. H.; Loo, J. S. C.; Cao, B.; Zhang, J. R.; Zhu, J. J.; Zhang, Q. C. Living and conducting: Coating individual bacterial cells with *in situ* formed polypyrrole. *Angew. Chem., Int. Ed.* **2017**, *56*, 10516–10520.

[25] Kaneko, M.; Ishihara, K.; Nakanishi, S. Redox-active polymers connecting living microbial cells to an extracellular electrical circuit. *Small* **2020**, *16*, 2001849.

[26] Liu, S. R.; Cai, L. F.; Wang, L. Y.; Yi, X. F.; Peng, Y. J.; He, N.; Wu, X. E.; Wang, Y. P. Polydopamine coating on individual cells for enhanced extracellular electron transfer. *Chem. Commun.* **2019**, *55*, 10535–10538.

[27] Vona, D.; Cicco, S. R.; Ragni, R.; Vicente-Garcia, C.; Leone, G.; Giangregorio, M. M.; Palumbo, F.; Altamura, E.; Farinola, G. M. Polydopamine coating of living diatom microalgae. *Photochem. Photobiol. Sci.* **2022**, *21*, 949–958.

[28] Cui, X. Q.; Xu, S. J.; Jin, C.; Ji, Y. B. Recent advances in the preparation and application of mussel-inspired polydopamine-coated capillary tubes in microextraction and miniaturized chromatography systems. *Anal. Chim. Acta* **2018**, *1033*, 35–48.

[29] Lee, H.; Dellatore, S. M.; Miller, W. M.; Messersmith, P. B. Mussel-inspired surface chemistry for multifunctional coatings. *Science* **2007**, *318*, 426–430.

[30] Wang, G. Y.; Huang, X. Y.; Jiang, P. K. Mussel-inspired fluoro-polydopamine functionalization of titanium dioxide nanowires for

polymer nanocomposites with significantly enhanced energy storage capability. *Sci. Rep.* **2017**, *7*, 43071.

[31] Buscemi, G.; Vona, D.; Labarile, R.; Ragni, R.; Milano, F.; Farinola, G. M.; Trotta, M. Ethylenediammine is not detrimental to the photoactivity of the bacterial photosynthetic reaction center. *MRS Adv.* **2021**, *6*, 265–269.

[32] Buscemi, G.; Vona, D.; Ragni, R.; Comparelli, R.; Trotta, M.; Milano, F.; Farinola, G. M. Polydopamine/ethylenediamine nanoparticles embedding a photosynthetic bacterial reaction center for efficient photocurrent generation. *Adv. Sustainable Syst.* **2021**, *5*, 2000303.

[33] Buscemi, G.; Vona, D.; Stufano, P.; Labarile, R.; Cosma, P.; Agostiano, A.; Trotta, M.; Farinola, G. M.; Grattieri, M. Bio-inspired redox-adhesive polydopamine matrix for intact bacteria biohybrid photoanodes. *ACS Appl. Mater. Interfaces* **2022**, *14*, 26631–26641.

[34] Labarile, R.; Varsalona, M.; Vona, D.; Stufano, P.; Grattieri, M.; Farinola, G. M.; Trotta, M. A novel route for anoxygenic polymerization of dopamine via purple photosynthetic bacteria metabolism. *MRS Adv.* **2023**, *8*, 423–428.

[35] Yu, Y. Y.; Wang, Y. Z.; Fang, Z.; Shi, Y. T.; Cheng, Q. W.; Chen, Y. X.; Shi, W. D.; Yong, Y. C. Single cell electron collectors for highly efficient wiring-up electronic abiotic/biotic interfaces. *Nat. Commun.* **2020**, *11*, 4087.

[36] Glaeser, J.; Klug, G. Photo-oxidative stress in *Rhodobacter sphaeroides*: Protective role of carotenoids and expression of selected genes. *Microbiology* **2005**, *151*, 1927–1938.

[37] Kushkevych, I.; Procházka, J.; Gajdács, M.; Rittmann, S. K. M. R.; Vítězová, M. Molecular physiology of anaerobic phototrophic purple and green sulfur bacteria. *Int. J. Mol. Sci.* **2021**, *22*, 6398.

[38] Tucker, J. D.; Siebert, C. A.; Escalante, M.; Adams, P. G.; Olsen, J. D.; Otto, C.; Stokes, D. L.; Hunter, C. N. Membrane invagination in *Rhodobacter sphaeroides* is initiated at curved regions of the cytoplasmic membrane, then forms both budded and fully detached spherical vesicles. *Mol. Microbiol.* **2010**, *76*, 833–847.

[39] D'Amici, G. M.; Rinalducci, S.; Murgiano, L.; Italiano, F.; Zolla, L. Oligomeric characterization of the photosynthetic apparatus of *Rhodobacter sphaeroides* R26.1 by nondenaturing electrophoresis methods. *J. Proteome Res.* **2010**, *9*, 192–203.

[40] Buccolieri, A.; Italiano, F.; Dell'Atti, A.; Buccolieri, G.; Giotta, L.; Agostiano, A.; Milano, F.; Trotta, M. Testing the photosynthetic bacterium *Rhodobacter sphaeroides* as heavy metal removal tool. *Ann. di Chim.* **2006**, *96*, 195–203.

[41] Ball, V. Polydopamine nanomaterials: Recent advances in synthesis methods and applications. *Front. Bioeng. Biotechnol.* **2018**, *6*, 109.

[42] Volpicella, M.; Costanza, A.; Palumbo, O.; Italiano, F.; Claudia, L.; Placido, A.; Picardi, E.; Carella, M.; Trotta, M.; Ceci, L. R. *Rhodobacter sphaeroides* adaptation to high concentrations of cobalt ions requires energetic metabolism changes. *FEMS Microbiol. Ecol.* **2014**, *88*, 345–357

[43] Papagiannakis, E.; Kennis, J. T. M.; van Stokkum, I. H. M.; Cogdell, R. J.; van Grondelle, R. An alternative carotenoid-to-bacteriochlorophyll energy transfer pathway in photosynthetic light harvesting. *Proc. Natl. Acad. Sci. USA* **2002**, *99*, 6017–6022.

[44] Zangmeister, R. A.; Morris, T. A.; Tarlov, M. J. Characterization of polydopamine thin films deposited at short times by autoxidation of dopamine. *Langmuir* **2013**, *29*, 8619–8628.

[45] Mehwish, N.; Xu, M. D.; Zaeem, M.; Lee, B. H. Mussel-inspired surface functionalization of porous albumin cryogels supporting synergistic antibacterial/antioxidant activity and bone-like apatite formation. *Gels* **2022**, *8*, 679.

[46] Reggente, M.; Roullier, C.; Mouhib, M.; Brandl, P.; Wang, H.; Tacconi, S.; Mura, F.; Dini, L.; Labarile, R.; Trotta, M. et al. Polydopamine-coated photoautotrophic bacteria for improving extracellular electron transfer in living photovoltaics. *Nano Res.* in press, https://doi.org/10.1007/s12274-023-6396-1.

[47] Salomaki, M.; Marttila, L.; Kivelä, H.; Ouvinen, T.; Lukkari, J. Effects of pH and oxidants on the first steps of polydopamine formation: A thermodynamic approach. *J. Phys. Chem. B* **2018**, *122*, 6314–6327.

[48] Červený, J.; Sinetova, M. A.; Zavřel, T.; Los, D. A. Mechanisms of high temperature resistance of *Synechocystis* sp. PCC 6803: An impact of histidine kinase 34. *Life* **2015**, *5*, 676–699